Simplified modeling of frequency behavior in photonic crystal vertical cavity surface emitting laser with tunnel injection quantum dot in active region

Mehdi Riahinasab[1,†], Vahid Ahmadi[2,‡], and Elham Darabi[3,§]

[1] Department of Electrical Engineering, Science and Research Branch, Islamic Azad University Tehran, Iran
[2] Department of Electrical Engineering, Tarbiat Modares University, Tehran, Iran
[3] Plasma Physics Research Center, Science and Research Branch, Islamic Azad University, Tehran, Iran

(Received 19 July 2016; revised manuscript received 17 October 2016; published online 10 January 2017)

In this work, the characteristics of the photonic crystal tunneling injection quantum dot vertical cavity surface emitting lasers (PhC-TIQD-VCSEL) are studied through analyzing a modified modulation transfer function. The function is based on the rate equations describing the carrier dynamics at different energy levels of dot and injector well. Although the frequency modulation response component associated with carrier dynamics in wetting layer (WL) and at excited state (ES) levels of dots limits the total bandwidth in conventional QD-VCSEL, our study shows that it can be compensated for by electron tunneling from the injector well into the dot in TIQD structure. Carrier back tunneling time is one of the most important parameters, and by increment of that, the bias current dependence of the total bandwidth will be insignificant. It is proved that at high bias current, the limitation of the WL-ES level plays an important role in reducing the total bandwidth and results in rollovers on 3-dB bandwidth-I curves. In such a way, for smaller air hole diameter of photonic crystal, the effect of this reduction is stronger.

Keywords: modulation transfer function, photonic crystal (PhC), tunnel injection quantum dot (TIQD), vertical cavity surface emitting laser (VCSEL)

PACS: 42.55.Px, 42.55.Tv **DOI:** 10.1088/1674-1056/26/2/024211

1. Introduction

Semiconductor quantum dot (QD) lasers including edge emitting and vertical cavity surface emitting lasers have more significant advantages than other lasers like bulk, quantum well, and wire in some characteristics, such as large differential gain,[1,2] low threshold current,[3,4] temperature insensitivity of the threshold current,[5,6] and high output power[7] because of their delta shape discrete density of states.

However, their carrier dynamic operations at high speed are not satisfactory enough, due to a phonon bottleneck appearing in electrons and holes capturing process[8,9] leading to a hot-carrier problem in QD lasers. The effect of hot carrier followed by the gain compression triggers the reduction of the differential gain.[10] Thus the resonance frequency is limited by the maximum modal gain and gain compression effects. Therefore the maximum modulation bandwidth, which is dependent on the resonance frequency and damping factor, decreases. So, the hot-carrier problem is an important reason for the disability of QD lasers to operate at high frequencies. Also, it is demonstrated that finite carrier capture, finite relaxation time, and Pauli blocking factors limit the maximum modulation bandwidth.[11]

To solve the problem one of the solutions is to use the tunneling injection method (TI). At first, the tunneling injection method is performed in active region for quantum well semiconductor lasers. By tunneling "cold" electrons directly into the lasing states of GaAs- and InP-based quantum well lasers from an adjacent injector layer, the performance characteristics including enhanced modulation bandwidth and higher characteristic temperature (T_0), the reduced Auger recombination and the reduced chirp are both demonstrated in Refs. [12]–[14]. Also, the TI scheme has been implemented in quantum well vertical-cavity surface-emitting lasers (QW-VCSELs).[15]

The technique of TI is applied to QD lasers, too. In tunneling injection quantum dot structure, electrons are introduced directly or in the phonon-assisted way into the lasing states of dots. Thus, the probabilities of electrons existing in the wetting layer and excited state, decrease. Then, the effects of hot carrier and gain compression are reduced and the differential gain increases.

By using the tunneling injection technique, small signal modulation is measured at frequencies more than 20 GHz.[16] In tunneling injection structure, in addition to the effect of carrier capture and relaxation, the tunneling rate also affects the

†E-mail: m.riahinasab@srbiau.ac.ir
‡Corresponding author. E-mail: v_ahmadi@modares.ac.ir
§E-mail: e.darabi@srbiau.ac.ir

© 2017 Chinese Physical Society and IOP Publishing Ltd

resonance frequency and damping factor. So, with a smaller tunneling time, the performance of laser is increased. It is shown in Ref. [17] that with different thickness values of the barrier, the tunneling time can be adjusted.

In this paper, a numerical model is presented to simulate the behavior of tunneling injection quantum dot VCSEL by using the method described in Ref. [11]. VCSELs are proven to have some unique properties such as high reliability, high internal efficiency, low divergence angle, simple fabrication process into twodimensional arrays.[18]

In our model, the bandwidths of modulation transfer functions associated with different levels of energy in dot and injector well are obtained. In this manner, the effect of tunnel injection on the resonance frequency and also on the bandwidth of modulation transfer function of TIQD laser is presented. Generally, the modulation transfer function components in the wetting layer (WL) and excited state (ES) limit the total bandwidth. However, in TIQD structure, modulation transfer function component related to tunneling process from injector well into QDs ground state experiences a high bandwidth leading to the increase of the entire modulation bandwidth. We base our study on the TI-QD-VCSEL model by a hetero-structure in active region and 1.3-μm QD-VCSEL which is based on experimental work in Refs. [19] and [20]. Also, in order to investigate the effect of photonic crystal (PhC) waveguide on the frequency behavior of laser, we consider a model of two-dimensional photonic crystal (PhC) waveguide embedded in entire VCSEL. The dynamic response of VCSEL varies with the structure and dimension of the laser cavity.[21] Oxide aperture depth and diameter as well as the characteristics of photonic crystal structure such as air holes diameter and PhC lattice constant are important parameters which affect the frequency response of VCSELs due to some properties such as spatial hole burning and self-heating effect. In order to take into account all phenomena of the laser, spatial hole burning (SHB) due to stimulated recombination of carriers and thermal lensing (TL) a result of the self-heating effect and transverse mode competition needs to be considered. The coupled optical field, diffusion, and thermal conduction equations are solved by using the algorithm of the self-consistent calculation which is described in Ref. [22].

The rest of this paper is organized as follows. In Sections 2 and 3, we investigate the dynamic carrier of the laser and the factors affecting the resonance frequency and damping factor and derive a new modulation transfer function similar to that in Ref. [11] through a small signal analysis of differential rate equations. In Section 4, the numerical results of tunneling injection are presented and by comparing with the conventional quantum dot, the origin of improvement of frequency response in TIQD structure, is investigated.

2. Structure

The schematic structure of the oxide-confined 1.3-μm QD-VCSEL is illustrated in Fig. 1. In this device, the active region is composed of ten self-assembled QD 6-nm InAs layers. The top and bottom mirrors consist of a 22-period p-type (doped 5×10^{17} cm^{-3}) and a 33-period n-type (doped 1×10^{18} cm^{-3}) quarter-wave GaAs-$Al_{0.9}Ga_{0.1}As$ layer distributed Bragg reflectors (DBR's), respectively. A 12-nm-thick AlAs layer embedded in the p-DBR adjacent to the active region is used for selective oxidation with oxide apertures of 10 μm–15 μm in diameter. The upper metal contact is fabricated on the top of the p-doped DBR and the bottom one on the n-doped substrate. Thickness values and compositions of all layers are presented in Ref. [23]. Also, we assume that the two-dimensional PhC waveguide embedded into VCSEL cavity has air-holes which go through the active region and both mirrors. Note that increasing the etching depth results in larger photonic crystal effect. The photonic crystal is composed of hexagonally arranged air-holes with diameter d_h and center-to center spacing A.

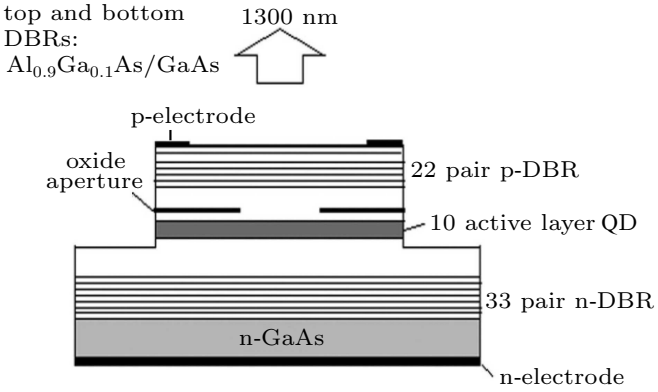


Fig. 1. Schematic diagram of the TIQD-VCSEL model.

3. Numerical model description

In the active region, we consider a model similar to the tunnel injection quantum dot active region structure in Ref. [16] whose sketch is shown in Fig. 2 consisting of the $In_{0.25}Ga_{0.75}As$ injector well, an $Al_{0.55}Ga_{0.45}As$ tunnel barrier, and three coupled $In_{0.25}Ga_{0.75}As$ QD layers. In order to efficiently realize the phonon assisted tunneling from the injector layer to the dots, the conduction band states of the injector layer with the bound states in QDs are aligned.[16] In our model, it is assumed that the active region consists of only one QD ensemble including two energy levels: a ground state (GS) with a two-fold degenerate and an excited state (ES) with a four-fold degeneration. The system is assumed to consist of excitonic energy states, while QDs are always neutral, and electrons and holes are treated as electron–hole pairs.

According to the carrier dynamics in the conduction band shown in Fig. 2, the external carriers are first injected into SCH and then into the injector well. Some of the carriers are then either introduced into the QD ground state directly or by phonon-assisted tunneling, and some of them participate in spontaneous emission processes, with a rate time of $\tau_{\text{spon-w}}$. Once in the WL, carriers are captured into the ES within time τ_{c1} and directly into the GS within time τ_{c0} or participate in spontaneous emission processes with a rate time of $\tau_{\text{spon-WL}}$. Carriers on the excited state are relaxed into the GS within time τ_{10} and on the other hand, they are also thermally reemitted from the ES to the WL with a τ_{e1} which is governed by the Fermi distribution for the quasi-thermal equilibrium without external excitation.[24] Carriers on the ground state level have a similar dynamic behavior to ES, while some of them recombine spontaneously with a spontaneous time τ_s. Most carriers reside in the injector well and in the wetting layer at room temperature, so the Auger recombination has not been explicitly considered in ES and GS levels.[16] In our model, the stimulated emission from the GS is just taken into account and occurs when the threshold is reached. Following the sketch in Fig. 2, the carrier dynamics defined by a set of rate equations given in Ref. [16] is as follows:

$$\frac{\mathrm{d}N_{\mathrm{w}}}{\mathrm{d}t} = \frac{J}{qd} + \frac{N_{\mathrm{w}}}{\tau_{\mathrm{tun}}}\cdot\left(1-\frac{N_{\mathrm{d0}}}{2N_{\mathrm{d}}}\right) + \frac{N_{\mathrm{d0}}}{\tau_{\mathrm{tunback}}} - \frac{N_{\mathrm{w}}}{\tau_{\text{spon-w}}}, \tag{1a}$$

$$\frac{\mathrm{d}N_{\mathrm{WL}}}{\mathrm{d}t} = -\frac{N_{\mathrm{WL}}}{\tau_{c1}}\cdot\left(1-\frac{N_{\mathrm{d1}}}{4N_{\mathrm{d}}}\right) + \frac{N_{\mathrm{d1}}}{\tau_{e1}} - \frac{N_{\mathrm{WL}}}{\tau_{c0}}\cdot\left(1-\frac{N_{\mathrm{do}}}{2N_{\mathrm{d}}}\right) + \frac{N_{\mathrm{d0}}}{\tau_{e0}} - \frac{N_{\mathrm{WL}}}{\tau_{\text{spon-WL}}}, \tag{1b}$$

$$\frac{\mathrm{d}N_{\mathrm{d1}}}{\mathrm{d}t} = -\frac{N_{\mathrm{d1}}}{\tau_{10}}\cdot\left(1-\frac{N_{\mathrm{d0}}}{2N_{\mathrm{d}}}\right) + \frac{N_{\mathrm{d0}}}{\tau_{01}}\cdot\left(1-\frac{N_{\mathrm{d1}}}{4N_{\mathrm{d}}}\right) - \frac{N_{\mathrm{d1}}}{\tau_{e1}} + \frac{N_{\mathrm{WL}}}{\tau_{c1}}\cdot\left(1-\frac{N_{\mathrm{d1}}}{4N_{\mathrm{d}}}\right), \tag{1c}$$

$$\frac{\mathrm{d}N_{\mathrm{d0}}}{\mathrm{d}t} = \frac{N_{\mathrm{W}}}{\tau_{\mathrm{tun}}}\cdot\left(1-\frac{N_{\mathrm{d0}}}{2N_{\mathrm{d}}}\right) - \frac{N_{\mathrm{d0}}}{\tau_{\mathrm{tunback}}} + \frac{N_{\mathrm{d1}}}{\tau_{10}}\cdot\left(1-\frac{N_{\mathrm{d0}}}{2N_{\mathrm{d}}}\right) + \frac{N_{\mathrm{WL}}}{\tau_{c0}}\cdot\left(1-\frac{N_{\mathrm{d0}}}{2N_{\mathrm{d}}}\right) - \frac{N_{\mathrm{d0}}}{\tau_{e0}} - \frac{N_{\mathrm{d0}}}{\tau_{01}}\cdot\left(1-\frac{N_{\mathrm{d1}}}{4N_{\mathrm{d}}}\right) - \frac{N_{\mathrm{d0}}}{\tau_{s}} - g\cdot v_{\mathrm{g}}\cdot S, \tag{1d}$$

$$\frac{\mathrm{d}S}{\mathrm{d}t} = \Gamma_{\mathrm{p}}\cdot g\cdot v_{\mathrm{g}}\cdot S - \frac{S}{\tau_{\mathrm{p}}} + \Gamma_{\mathrm{p}}\cdot\beta_{\mathrm{sp}}\cdot\frac{N_{\mathrm{d0}}}{\tau_{s}}, \tag{1e}$$

where N_{w}, N_{WL}, N_{d1}, and N_{d0} are the carrier densities in the injector well, the wetting layer, the excited state of dots, and the ground state, respectively; S is the photon density in the cavity; β_{sp} and Γ_{p} are the spontaneous emission and optical confinement factors; τ_{p} is the photon lifetime; v_{g} is the group velocity. Definitions of some parameters and displayed time constants in Fig. 1 are listed in Table 1.[11,16,23]

Table 1. Some laser parameters and time constants.

Parameter	Symbol	Value	Unit
Capture time from WL to ES	τ_{c1}	7	ps
Capture time from WL to GS	τ_{c0}	15	ps
Relaxation time from ES to GS	τ_{10}	5–13	ps
Tunneling time to GS	τ_{tun}	1–2	ps
Capture time to WL	τ_{WL}	1.7	ps
Spontaneous emission factor	β_{sp}	1×10^{-8}	–
Optical confinement factor	Γ_{p}	0.06	–
Radiative recombination time	τ_{s}	2	ns
Group velocity	v_{g}	8.5×10^{7}	m/s
Photon lifetime	τ_{p}	12	ps
Spontaneous emission time of WL	$\tau_{\text{spon-WL}}$	400	ps
Spontaneous emission time of well	$\tau_{\text{spon-w}}$	400	ps

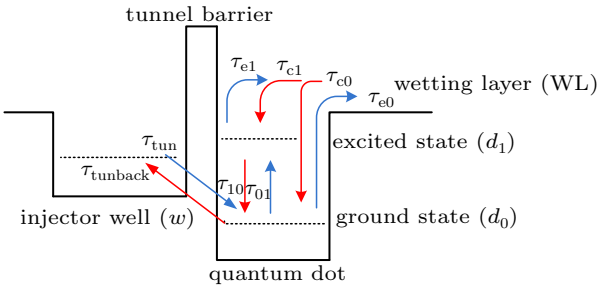


Fig. 2. (color online) Transport processes in the active region of TIQD laser.

The probabilities to find an empty carrier state on the GS and ES levels (f_{gs} and f_{es}) which are known as the Pauli blocking factors, are defined as

$$f_{\mathrm{gs}} = 1-\frac{N_{\mathrm{d0}}}{2N_{\mathrm{d}}} \quad \text{and} \quad f_{\mathrm{es}} = 1-\frac{N_{\mathrm{d1}}}{4N_{\mathrm{d}}}. \tag{2}$$

The optical gain in the cavity as a function of N_{d0} and S is given by

$$g = g_0\cdot N_{\mathrm{d}}\cdot\left(\frac{N_{\mathrm{d0}}}{N_{\mathrm{d}}}-1\right)\cdot\frac{1}{1+\varepsilon S}, \tag{3}$$

where N_{d} is the total QD number, g_0 is the differential gain, and ε is the gain compression factor representing the variation of optical gain with the photon density. The gain variation as a dynamic variable with carrier and photon density is defined as

$$\mathrm{d}g = g_0\,\mathrm{d}N_{\mathrm{d0}} - g_{\mathrm{s}}\,\mathrm{d}S,$$

where $g_0 = \partial g/(\partial N_{\mathrm{d0}})$ and $g_{\mathrm{s}} = -\partial g/(\partial S)$.

Instead of g_{s}, one can often use the gain compression factor ε to describe the gain dependence on photon density.[10] In Eq. (3), ε is thus related to g_{s} by $g_{\mathrm{s}} = \varepsilon g/(1+\varepsilon g)$. It should be noted that the differential gain g_0 and the gain compression factor ε are well-defined physical quantities in that their values are derived from device characteristics. In contrast, the optical gain g and the gain derivative versus photon number g_{s} are not uniquely defined in QDs, since their values need to be calculated by considering the radius dependence of carrier concentration.[10]

By utilizing the definition of the small-signal form of the dynamic variables including I, N_{w}, N_{WL}, N_{d1}, N_{d0}, and g and

by deriving the differential rate equations, the matrix form of rate equations for a small-signal response to a sinusoidal current modulation with the modulation frequency $\omega/2\pi$, is obtained as follows:

$$\begin{bmatrix} j\omega+\gamma_{11} & -\gamma_{12} & 0 & -\gamma_{14} & 0 \\ -\gamma_{21} & j\omega+\gamma_{22} & -\gamma_{23} & -\gamma_{24} & 0 \\ 0 & -\gamma_{32} & j\omega+\gamma_{33} & -\gamma_{34} & 0 \\ -\gamma_{41} & -\gamma_{42} & -\gamma_{43} & j\omega+\gamma_{44} & -\gamma_{45} \\ 0 & 0 & 0 & -\gamma_{54} & j\omega+\gamma_{55} \end{bmatrix} \cdot \begin{bmatrix} N_w \\ N_b \\ N_{d1} \\ N_{d0} \\ S \end{bmatrix} = \frac{I}{qd} \cdot \begin{bmatrix} 1 \\ 0 \\ 0 \\ 0 \\ 0 \end{bmatrix} \tag{4}$$

with

$$\begin{aligned} &\gamma_{11} = \frac{f_{gs}}{\tau_{tun}} + \frac{1}{\tau_{spon_w}};\ \ \gamma_{12} = 0; \\ &\gamma_{14} = \frac{1}{\tau_{tunback}};\ \ \gamma_{21} = 0; \\ &\gamma_{22} = \frac{f_{es}}{\tau_{c1}} + \frac{f_{gs}}{\tau_{c0}} + \frac{1}{\tau_{spon_WL}}; \\ &\gamma_{23} = \frac{1}{\tau_{e1}};\ \ \gamma_{24} = \frac{1}{\tau_{e0}};\ \ \gamma_{32} = \frac{f_{es}}{\tau_{c1}}; \\ &\gamma_{33} = \frac{f_{gs}}{\tau_{10}} + \frac{1}{\tau_{e1}};\ \ \gamma_{34} = \frac{f_{es}}{\tau_{01}}; \\ &\gamma_{41} = \frac{f_{gs}}{\tau_{tun}};\ \ \gamma_{42} = \frac{f_{gs}}{\tau_{c0}};\ \ \gamma_{43} = \frac{f_{gs}}{\tau_{10}}; \\ &\gamma_{44} = \frac{1}{\tau_{tunback}} + \frac{1}{\tau_{e0}} + \frac{f_{es}}{\tau_{01}} + \frac{1}{\tau_s} + v_g \cdot g_0 \cdot S; \\ &\gamma_{45} = v_g \cdot g_s \cdot S - v_g \cdot g; \\ &\gamma_{54} = \frac{\Gamma_p \cdot \beta_{sp}}{\tau_s} + \Gamma_p \cdot v_g \cdot g_0 \cdot S; \\ &\gamma_{55} = \Gamma_p \cdot v_g \cdot g_s \cdot S - \Gamma_p \cdot v_g \cdot g + \frac{1}{\tau_p}. \end{aligned} \tag{5}$$

As given in Ref. [11], one can extract a modulation transfer function as

$$H_{TIQD} = \frac{R_0}{\Delta} = \frac{R_0}{j\omega^5 + R_4\omega^4 - R_3 j\omega^3 - R_2\omega^2 + R_1 j\omega + R_0}, \tag{6}$$

where Δ is the determinant of the matrix symbol and the R parameters can be obtained from the coefficients of the matrix.

Now, we define the relaxation resonance frequency and damping factor for the lasing level versus coefficients of matrix as

$$\omega_R^2 = \gamma_{44}\gamma_{55} - \gamma_{45}\gamma_{54}, \tag{7a}$$

$$\Gamma = \gamma_{44} + \gamma_{55}, \tag{7b}$$

and for carrier relaxation and capture levels as

$$\omega_{R_0}^2 = \gamma_{22}\gamma_{33} - \gamma_{23}\gamma_{32}, \tag{8a}$$

$$\Gamma_0 = \gamma_{22} + \gamma_{33}. \tag{8b}$$

By eliminating the insignificant components of R parameters, their definitions can be simplified into

$$R_0 = \gamma_{11}\omega_R^2\omega_{R_0}^2 - \gamma_{12}\gamma_{21}\gamma_{33}\omega_R^2, \tag{9a}$$

$$R_1 = \gamma_{12}\gamma_{21}\gamma_{33}\omega_R^2 - \gamma_{12}\gamma_{21}\gamma_{33}\Gamma + \gamma_{11}\Gamma\omega_{R_0}^2 + \gamma_{11}\Gamma_0\omega_R^2 + \omega_R^2\omega_{R_0}^2, \tag{9b}$$

$$R_2 = \gamma_{11}\omega_{R_0}^2 + \gamma_{11}\Gamma\Gamma_0 + \omega_{R_0}^2\Gamma + \omega_R^2 \cdot (\gamma_{11} + \Gamma) - \gamma_{12}\gamma_{21} \cdot (\gamma_{33} + \Gamma), \tag{9c}$$

$$R_3 = \gamma_{11} \cdot (\Gamma + \Gamma_0) + \Gamma\Gamma_0 + \omega_R^2 + \omega_{R_0}^2 - \gamma_{12}\gamma_{21}, \tag{9d}$$

$$R_4 = \gamma_{11} + \Gamma + \Gamma_0. \tag{9e}$$

Based on these simplifications, the modulation transfer function (6) will be approximated and rewritten as:

$$H_{app}(\omega) = H_{stim}(\omega) \cdot H_{WL\text{-}ES}(\omega) \cdot H_{tun}(\omega), \tag{10a}$$

where

$$H_{stim}(\omega) = \frac{\omega_R^2}{\omega_R^2 - \omega^2 + j\omega\Gamma}, \tag{10b}$$

$$H_{WL\text{-}ES}(\omega) = \frac{\omega_{R_0}^2}{\omega_{R_0}^2 - \omega^2 + j\omega\Gamma_0}, \tag{10c}$$

$$H_{tun}(\omega) = \frac{\gamma_{11}}{j\omega + \gamma_{11}}. \tag{10d}$$

Here, $H_{stim}(\omega)$ is the expression of modulation transfer function for lasing; $H_{WL\text{-}ES}(\omega)$ and $H_{tun}(\omega)$are the modulation transfer functions in WL-ES levels and tunneling process from injector well into QDs ground states. As shown, the parameters affecting on the behavior of modulation transfer function $H(\omega)$ are constant times in WL, ES, and GS, tunneling time into the WL and GS as well as Pauli blocking factors of the GS and ES.

The relaxation resonance frequency (ω_R) and damping factor (Γ) can be obtained by using the set of γs parameters and utilizing the steady state relationship for photon equation as follows:

$$\omega_R^2 = \frac{v_g g_0 S}{\tau_p} + \left(\frac{1}{\tau_{tunback}} + \frac{1}{\tau_{e0}} + \frac{f_{es}}{\tau_{01}} + \frac{1-\beta_{sp}}{\tau_s}\right) \times \left(\frac{\Gamma_p \beta_{sp} N_{d0}}{\tau_s S} + \Gamma_p v_g g_s S\right) + \frac{\beta_{sp}}{\tau_s \tau_p}, \tag{11}$$

$$\Gamma = v_g g_0 S\left(1 + \frac{\Gamma_p g_s}{g_0}\right) + \frac{1}{\tau_{tunback}} + \frac{1}{\tau_{e0}} + \frac{f_{es}}{\tau_{01}} + \frac{1}{\tau_s} + \frac{\Gamma_p \beta_{sp} N_{d0}}{\tau_s S}. \tag{12}$$

These equations are the same as those obtained from Ref. [11] in terms of f_{es}/τ_{01} which denotes the carrier escaping from the GS to ES, but there is an additional term of $1/\tau_{tunback}$ which represents the carrier back tunneling from the GS to the injector well. This discrepancy causes some behaviors of ω_R^2 and Γ to be different from those in the conventional QDs. It is important to investigate these differences and their origins. Physical origin of back tunneling time can be explained

as follows. Generally, the tunneling component of carriers from injector well into the QDs is $W_{\rm n}N_{\rm d}(1-f_{\rm gs})N_{\rm w}$, and the back tunneling component of carriers from the QDs into the injector well is $W_{\rm n}n^{\rm QD}N_{\rm d}f_{\rm gs}$. $W_{\rm n}$ is tunneling coefficient (in units of $\rm cm^3/s$ for carrier tunneling between the QD ensemble and the QW. This tunneling coefficient is primarily controlled by the thickness and material parameters of the barrier, and also by the QD and QW parameters which in a properly designed structure should be small. $n^{\rm QD}$ (in units of $\rm cm^{-3}$) is the density of carriers in the tunneling flux from the QD ensemble to the injector well which depends on carrier density in the injector well $(N_{\rm w})$, the Pauli blocking factor in the GS $(f_{\rm gs})$. Under thermal equilibrium for the tunneling process from the injector well to QDs $(W_{\rm n}N_{\rm d}(1-f_{\rm gs})N_{\rm w})$ and from QDs to the injector well $(W_{\rm n}n^{\rm QD}N_{\rm d}f_{\rm gs})$, $n^{\rm QD}$ is equal to $N_{\rm w}(1-f_{\rm gs})/f_{\rm gs}$. So, by using our expressions for back tunneling process in rate equations, the back tunneling time can be defined as $\tau_{\rm tunback}=N_{\rm d0}/(W_{\rm n}n^{\rm QD}N_{\rm d}f_{\rm gs})$.

Due to the relationships obtained for the resonance frequency and damping factor in lasing and relaxation environments, it can be seen that in addition to the all constant times, some parameters such as gain (g), the photon density (S), carrier density in ES and GS and subsequently their Pauli blocking factors affect the frequency behavior of laser. These parameters also are dependent on the operation and structure of laser such as the active region and the characteristics of photonic crystal structure. So, to calculate accurately the parameters and consider the effects of spatial hole burning (SHB) and thermal lensing (TL), it is necessary to solve the coupled equations of optical field, carrier concentration, and thermal at all points of the radial active region of the VCSEL. The coupled equations which we consider in our model, are as follows.

Scalar Helmholtz equation which describes transverse mode distribution E can be written as

$$\nabla^2 E(x,y)+\left\{n^2(x,y)k_0^2-\beta^2\right\}E(x,y)=0, \tag{13}$$

where $E(x,y)$ is the transverse electrical field pattern, $n(x,y)$ is the refractive index pattern, $k_0=2\pi/\lambda$ is vacuum preparation constant, λ is the wavelength of optical wave, $\beta=n_{\rm m}k_0$ is the mode propagation constant, and $n_{\rm m}$ is the mode effective index. The transverse distribution of the refractive index can be defined as follows:

$$n(x,y)=\begin{cases} n_{\rm r}+{\rm j}\dfrac{g\lambda}{4\pi}, & r\le s;\\ n_{\rm r}-\Delta n_{\rm r}, & r\ge s;\\ 1, & \text{for holes,}\end{cases} \tag{14}$$

where $n_{\rm r}$ is the refractive index of passive GaAs region, g is described in Eq. (3) and depends on radial profile of carrier density, and s is the radius of the oxide aperture. Taking into account the spatial hole burning (SHB) and thermal lensing (TL) effects, we consider the contributions of carrier and temperature distributions to changes of the refractive index $\Delta n_{\rm r}$,

$$\Delta n_{\rm r}=\frac{\partial n_{\rm r}}{\partial N}\Delta N+\frac{\partial n_{\rm r}}{\partial T}\Delta T, \tag{15}$$

with $\partial n_{\rm r}/\partial N=-q^2/(2n_0\varepsilon_0\omega^2 m_{\rm n})$, where n_0 is the refractive index of active region, and $m_{\rm n}$ is the effective mass of the electron.

For GaAs,

$$\frac{\partial n_{\rm r}}{\partial T}\cong 4\times10^{-4}\left({\rm K}^{-1}\right).$$

By neglecting the temperature variation in the longitudinal direction, the thermal conduction equation in steady state is given by,

$$\frac{1}{r}\frac{\partial}{\partial r}\left(r\frac{\partial T}{\partial r}\right)+\frac{1}{\lambda_i}Q(J,r)=0, \tag{16}$$

where T is the temperature, λ_i is the effective thermal conductivity of the laser cavity, r denotes radius, $Q(J,r)$ is the density of the total heat energy generated in the laser including Joule heating in DBR layers, absorption of spontaneous emission, and nonradiative recombination in the active region. We calculate $Q(J,r)$ by following the approach in Ref. [23]. The most significant current spreading in the VCSEL takes place in the current region. To simplify the calculation, we consider the following approximation:

$$J(r)=\begin{cases} J_0, & r\le s;\\ J_0\exp\left(\dfrac{-(r-s)}{r_0}\right), & r\ge s,\end{cases} \tag{17}$$

where J_0 is the injected current density and r_0 is a constant which determines the extent of the current spreading.

4. Results and discussion

At first, we numerically solve the steady state of the coupled equations (13)–(17) by using the algorithm of the self-consistent calculation. Diffusion equations of TIQD structure are created from the rate equation with adding $\nabla^2 N_{\rm w}$ and $\nabla^2 N_{\rm WL}$ terms in steady state and is solved with the nonlinear Newton method for determining the radial profile of carrier concentration. Thermal equation is solved by the finite difference method with Dirichlet boundary conditions. Field equation is solved by the finite difference method with absorbing boundary conditions accordingly to $(\nabla-{\rm j}n(x,y)k_0)E_j(x,y)=0$. Then, the frequency behavior of laser is studied by using an analytical approximation of the model which has been discussed in the previous section.

The components of approximate solution $H_{\rm app}(\omega)$ presented in Eqs. (10a)–(10d) are shown in Fig. 3. The inset presents the precise modulation transfer function $H_{\rm TIQD}(\omega)$ given by Eq. (6) and the approximate solution $H_{\rm app}(\omega)$ which

shows that the $H_{\mathrm{TIQD}}(\omega)$ and $H_{\mathrm{app}}(\omega)$ curves are approximately close to each other.

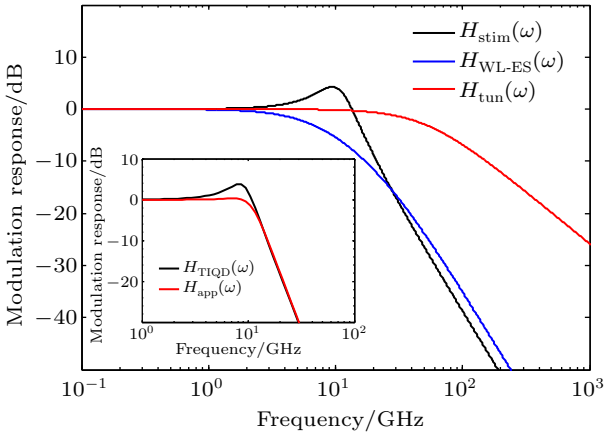


Fig. 3. (color online) Components of approximate solution $H_{\mathrm{app}}(\omega)$. The inset shows precise modulation transfer function $H_{\mathrm{TIQD}}(\omega)$ and the approximate solution $H_{\mathrm{app}}(\omega)$ for TIQD-VCSEL.

It can be seen that the behavior of response of $H_{\mathrm{stim}}(\omega)$ to frequency is similar to that of quantum well structure.[11] While, among the components of $H_{\mathrm{app}}(\omega)$, $H_{\mathrm{WL\text{-}ES}}(\omega)$ is the underlying limitation to the enhancement of the total modulation bandwidth, because the modulation bandwidth of $H_{\mathrm{WL\text{-}ES}}(\omega)$ is much smaller than others'. Of course, in TIQD structure, the carrier dynamics in the inter-band of dots has no significant influence on $H_{\mathrm{WL\text{-}ES}}(\omega)$, while in CQD, the finite carrier capture time and finite carrier relaxation time are the effective physical limitations to the enhancement of $H_{\mathrm{WL\text{-}ES}}(\omega)$ modulation bandwidth.[11] This is the evidence for the advantage of using a tunnel injection quantum dot compared with using the conventional QD. In addition, $H_{\mathrm{tun}}(\omega)$ has the highest bandwidth, which leads to the increase of the total modulation bandwidth. Given that this component is related to the tunneling time, the behavior of modulation will be improved for shorter tunneling time.

Generally, due to tunnelling injection, total frequency behaviour of laser has less dependence on inter-band dynamic of QD. However, the back tunnelling time from GS to the injector well is a more important parameter for determining the 3-dB bandwidth of total transfer function by its direct influence on the bandwidth of $H_{\mathrm{stim}}(\omega)$. Figure 4 shows frequency responses of the laser for four different values of back tunnelling time from GS to the injector well (τ_{tunback}) at $1.2I_{\mathrm{th}}$, while the inset shows $f_{3\ \mathrm{dB}}$ variations of $H_{\mathrm{stim}}(\omega)$ with τ_{tunback} for differentvalues of carrier tunnelling time (τ_{tun}). By comparing these results, it can be seen that by increasing the τ_{tunback}, $f_{3\ \mathrm{dB}}$ of total transfer function is increased due to high increment of $f_{3\ \mathrm{dB}}$ of $H_{\mathrm{stim}}(\omega)$ as shown in the inset. As depicted, in the case of low back tunnelling time, the changes of 3-dB bandwidth of $H_{\mathrm{stim}}(\omega)$ is intense, but in the case of high value of back tunnelling time, 3-dB bandwidth of $H_{\mathrm{stim}}(\omega)$ changes slower so that, forshort tunneling time, it is approximately independent of τ_{tunback}. Also, with small back tunnelling time, τ_{tun} has an indirect influence on the bandwidth of lasing transfer function component $H_{\mathrm{stim}}(\omega)$ due to generated photon. While, in the case of large back tunnelling time, the effect of τ_{tun} on the bandwidth of $H_{\mathrm{stim}}(\omega)$ is very weak. Because, by increasing τ_{tunback}, there will be no back tunneling process approximately toward injector well. So, carrier densities at the ES and the GS levels of dots as well as the Pauli blocking factors $(f_{\mathrm{gs}}, f_{\mathrm{es}})$ have small changes due to photon density created in the cavity and will almost be less dependent on the value of τ_{tun}. According to the expressions of ω_{R}^2 and Γ in $H_{\mathrm{stim}}(\omega)$ and their dependence on photon density, 3-dB bandwidth of $H_{\mathrm{stim}}(\omega)$ is less impressible to τ_{tun} for large value of τ_{tunback}.

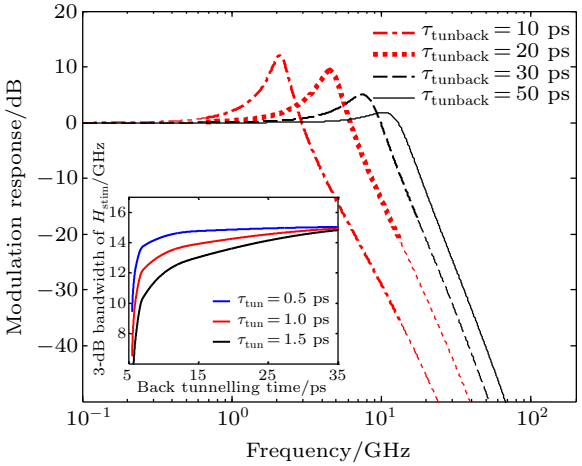


Fig. 4. (color) Frequency responses of TIQD-VCSEL for four values of τ_{tunback}. The inset shows $f_{3\ \mathrm{dB}}$ variations of $H_{\mathrm{stim}}(\omega)$ with τ_{tunback} for different values of τ_{tun}.

The frequency response of the laser is plotted in Fig. 5 for two different values of back tunnelling time (τ_{tunback}) at $1.1I_{\mathrm{th}}$ and $1.5I_{\mathrm{th}}$. It can be concluded that for a large value of τ_{tunback}, the dependence of 3-dB bandwidth on the bias current is not so strong. The inset shows laser 3-dB bandwidth changes of $H_{\mathrm{stim}}(\omega)$ with bias current for three different values of τ_{tunback}. It is observed that by increasing τ_{tunback},

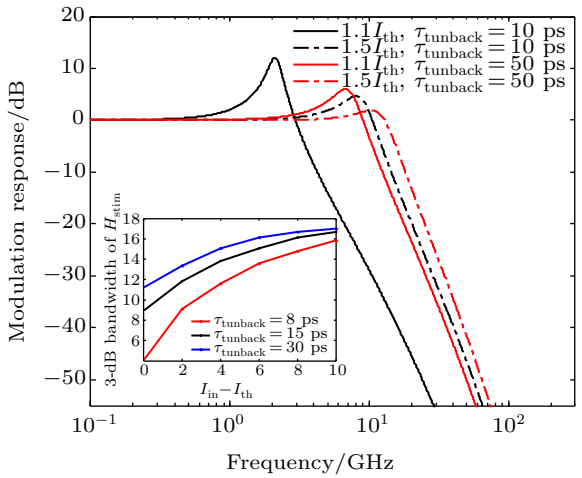


Fig. 5. (color online) Frequency responses of TIQD-VCSEL for two values of τ_{tunback} at $1.1I_{\mathrm{th}}$ and $1.5I_{\mathrm{th}}$. The inset shows $f_{3\ \mathrm{dB}}$ variations of $H_{\mathrm{stim}}(\omega)$ with bias current for three values of τ_{tunback}.

the dependence of $f_{3\ \mathrm{dB}}$ on the bias current decreases with the increase of current. It should be noted that the bandwidth of $H_{\mathrm{WL\text{-}ES}}(\omega)$ is not dependent on τ_{tun}, nor τ_{tunback}. But, the tunnelling time τ_{tun} affects the bandwidth of $H_{\mathrm{tun}}(\omega)$ strongly.

Now, in order to investigate the effect of photonic crystal (PhC) waveguide on the frequency behavior of laser, the 3-dB bandwidth of transfer function of TIQD-PhC-VCSEL and its components are plotted in Figs. 6(a)–6(c) as a function of injected current for various values of air hole diameter (d_{h}) with a fixed value of PhC lattice constant ($A = 2$ μm). Oxide aperture diameter (s) and spreading current (r) are 10 μm and 1 μm, respectively. The threshold currents are obtained to be 3.2 mA, 4.6 mA, and 59 mA. The 3-dB bandwidth of transfer function of TIQD-VCSEL with the same structure is shown in the inset of Fig. 6(a). As can be seen from Fig. 6(a) the bandwidth of $H_{\mathrm{TIQD}}(\omega)$ increases with increasing bias current and is saturated for high values. The occurrence of rollover of the modulation response at the high bias current is due to both self-heating effect (with more effectiveness) and the emergence of high-order modes (with less effectiveness). The rollovers are observed at $f_{3\ \mathrm{dB}} = 11.6$ GHz for $d_{\mathrm{h}}/A = 0.2$, $f_{3\ \mathrm{dB}} = 12.4$ GHz for $d_{\mathrm{h}}/A = 0.4$, and $f_{3\ \mathrm{dB}} = 13.5$ GHz for $d_{\mathrm{h}}/A = 0.6$, respectively. While in TIQD-VCSEL without photonic crystal structure the rollover is at $f_{3\ \mathrm{dB}} = 11.15$ GHz at 3.4-mA threshold current. Relaxation rate in QD will decrease as a result of phonon bottleneck caused by increasing temperature in the active region. For larger air hole diameter, the bandwidth increases more intensely at low bias currents, and is saturated later. Since the air holes diameter has a significant influence on the reduction of thermal lensing and spatial hole burning effect. So, with its increase, the temperature decreases and the gain increases in the center of the active region. In TIQD structures, this rollover is less than that in conventional quantum dot structure by solving the phonon bottleneck problem. In order to further analyse the variations of 3-dB bandwidth of $H_{\mathrm{stim}}(\omega)$ and $H_{\mathrm{WL\text{-}ES}}(\omega)$ versus bias current are shown in Figs. 6(b)–6(c). The presented results point out that 3-dB bandwidth of $H_{\mathrm{stim}}(\omega)$ increases with the increase of current, while $f_{3\ \mathrm{dB}}$ of $H_{\mathrm{WL\text{-}ES}}(\omega)$ is reduced, slightly. The effect of air-hole diameter on the 3-dB bandwidth of $H_{\mathrm{stim}}(\omega)$ is almost similar to that of $H_{\mathrm{TIQD}}(\omega)$. The reduction of 3-dB bandwidth of $H_{\mathrm{WL\text{-}ES}}(\omega)$ is more intense for smaller air-hole diameter. Based on the variations of $H_{\mathrm{stim}}(\omega)$ and $H_{\mathrm{WL\text{-}ES}}(\omega)$ as well as $H_{\mathrm{TIQD}}(\omega)$, in the case of low bias current the effect of increase of 3-dB bandwidth of $H_{\mathrm{stim}}(\omega)$ is dominant over the effect of reduction of 3-dB bandwidth of $H_{\mathrm{WL\text{-}ES}}(\omega)$, while frequency behavior of $H_{\mathrm{WL\text{-}ES}}(\omega)$ will be predominant in the case of high bias current. On the other hand, carrier dynamic behaviors in wetting layer and excited state levels are more influenced by spatial hole burning and thermal effects. In the TIQD structures, current dependence of ω_{R0}^2 and Γ are negligible despite CQD decreasing linearly with the increase of current.[11] Thus, the limitation to the bandwidth of $H_{\mathrm{WL\text{-}ES}}(\omega)$ does not restrict the total modulation bandwidth with the increase of current. This is attributed to the current being not dependent on Pauli blocking factor f_{es} nor f_{gs}. The $f_{3\ \mathrm{dB}}$ of $H_{\mathrm{tun}}(\omega)$ is approximately independent of the current (not shown here). Based on Eqs. (5) and (10d), the results indicate that the constant Pauli blocking factor in ground state (f_{gs}) is effective to small reduction of 3-dB bandwidth of $H_{\mathrm{tun}}(\omega)$ in TIQD when increasing the current.

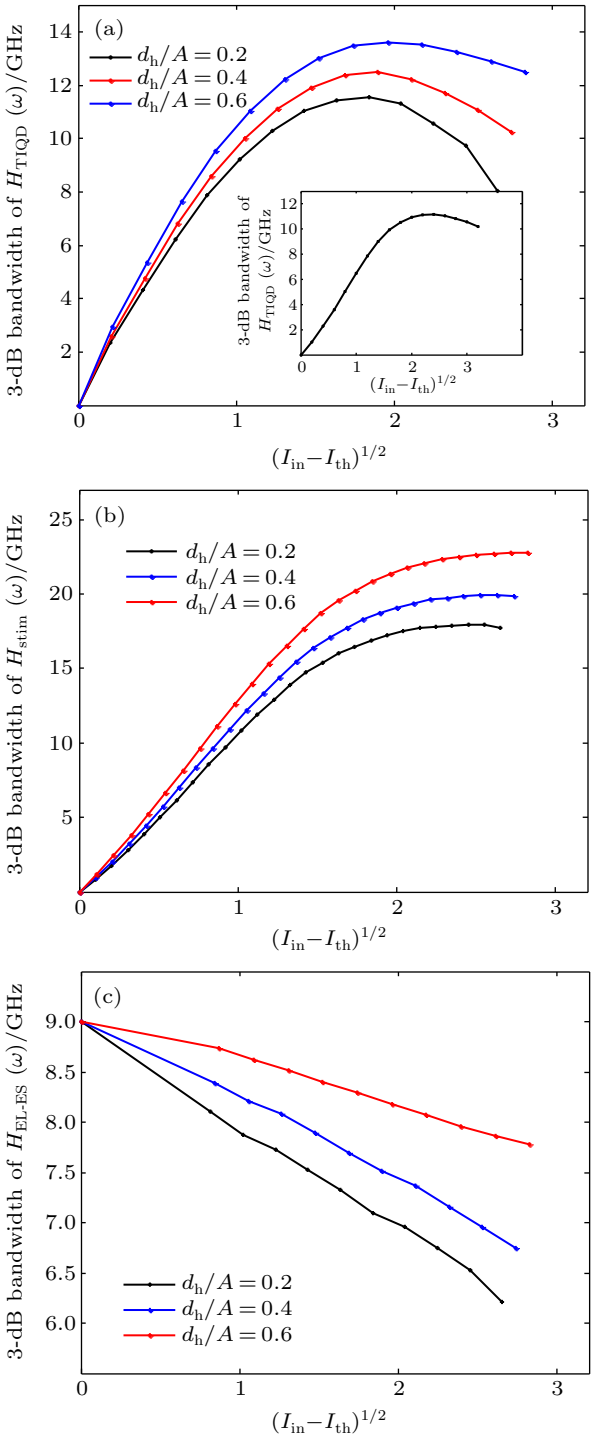


Fig. 6. (color online) Plots of 3-dB frequency of approximation modulation transfer function with its components versus $(I–I_{\mathrm{th}})^{1/2}$ for various values of air-hole diameter (d_{h}) with $A = 2$ μm in TIQD-PhC-VCSEL.

5. Conclusions

Through the analysis of modulation transfer function, the characteristics of the photonic crystal tunneling injection quantum dot vertical cavity surface emitting lasers (PhC-TIQD-VCSEL) are studied. Based on the rate equations describing the carrier dynamics, the modulation transfer function is obtained and divided into the components related to the energy levels in the dot and the injector well. Numerical investigation clarifies the effect of the tunneling injection on the enhancement of the modulation response. The results show that the carrier back-tunneling time from the dot ground state into the injector well is the most effective parameter to determine the frequency response of TIQD-VCSEL. The frequency behaviors of WL-ES and GS levels are also affected by the variations of the structure and dimension of laser cavity as well as air-hole diameter and lattice constant of photonic crystal structure due to some nonlinear effects such as spatial hole burning and thermal lensing effects. However the component of tunneling process is almost independent of them.

References

[1] Kirstaedter N, Schmidt O G, Ledentsov N N, Bimberg D, Ustinov V M, Egorov A, Zhukov A E, Maximov M V, Kopev P S and Alferov Z 1996 *Appl. Phys. Lett.* **69** 1226

[2] Klotzkin D, Kamath K, Vineberg K, Bhattacharya P, Murty R and Laskar J 1998 *IEEE Photon. Technol. Lett.* **10** 932

[3] Liu G T, Stintz A, Li H, Malloy K J and Lester L F 1999 *Electron. Lett.* **35** 1163

[4] Sarzala R P 2004 *IEEE J. Quantum Electron.* **40** 629

[5] Maksimov M V, Gordeev N Y, Zaitsev S V, Kop'ev P S, Kochnev I V, Ledentsov N N, Lunev A V, Ruvimov S S, Sakharov A V, Tsatsul'nikov A F, Shernyakov Y M, Alferov Z I and Bimberg D 1997 *Semiconductors* **31** 124

[6] Shchekin O B and Deppe D G 2002 *Appl. Phys. Lett.* **80** 3277

[7] Bimberg D, Grundmann M, Heinrichsdorff F, Ledentsov N N, Ustinov V M, Zhukov A E, Kovsh A R, Maximov M V, Shernyakov Y M and Volovik B V 2000 *Thin Solid Films* **367** 235

[8] Yavari M H and Ahmadi V 2011 *IEEE J. Sel. Top. Quantum Electron.* **17** 1153

[9] Razmpa Mand Emami F 2015 *Quantum Electronics* **45** 15

[10] Fiore A and Markus A 2007 *IEEE J. Quantum Electron.* **43** 287

[11] Wang C, Grillot F and Even J 2012 *IEEE J. Quantum Electron.* **48** 1144

[12] Bhattacharya P, Singh J, Yoon H, Zhang X, Gutierrez-Aitken A and Lam Y 1996 *IEEE J. Quantum Electron.* **32** 1620

[13] Zhang X, Gutierrez-Aitken A, Klotzkin D, Bhattacharya P, Caneau C and Bhat R 1997 *IEEE J. Sel. Top. Quantum Electron.* **3** 309

[14] Yoon H, Gutierrez-Aitken A L, Jambunathan R, Singh J and Bhattacharya P K 1995 *IEEE Photon. Technol. Lett.* **7** 974

[15] Huffaker D L and Deppe D G 1997 *Appl. Phys. Lett.* **71** 1449

[16] Bhattacharya P, Ghosh S, Pradhan S, Singh J, Wu Z K, Urayama J, Kim K and Norris T B 2003 *IEEE J. Quantum Electron.* **39** 952

[17] Cerulo G, Nevou L, Liverini V, Castellano F and Faist J 2012 *J. Appl. Phys.* **112** 43702

[18] Wang W J, Li C, Zhou H Y, Wu H, Luan X X, Shi L and Guo X 2015 *Chin. Phys. B* **24** 024209

[19] Tong C Z, Xu D W, Yoon S F, Ding Y and Fan W J 2009 *IEEE J. Sel. Top. Quantum Electron.* **15** 743

[20] Ding Y *et al.* 2010 in *Proc. SPIE-OSA-IEEE* **7631** 763102

[21] Yu S F 1996 *IEEE J. Quantum Electron.* **32** 1168

[22] Zhao Y G and Mcinerney J G 1996 *IEEE J. Quantum Electron.* **32** 1950

[23] Abbaspour H, Ahmadi V and Yavari M H 2011 *IEEE J. Sel. Top. Quantum Electron.* **17** 1327

[24] Grillot F, Veselinov K, Gioannini M, Montrosset I, Even J, Piron R, Homeyer E and Loualiche S 2009 *IEEE J. Quantum Electron.* **45** 872